

## **Inter-annual sea level variability in the southern South China Sea**

Soumya Mohan <sup>a</sup>, P. Vethamony <sup>a,\*</sup>, P. Tkalich <sup>b</sup>

<sup>a</sup>CSIR-National Institute of Oceanography, Dona Paula, Goa-403 004, India

<sup>b</sup>Tropical Marine Science Institute, National University of Singapore, 14 Kent Ridge Road, 119 227

\* **Corresponding author:** P. Vethamony, Email: mony@nio.org, Tel: +91832 2450473, Fax: +91832 2450608

### **Abstract**

The South China Sea (SCS) is the largest marginal sea in the western Pacific Basin. Sea level anomalies (SLAs) in the southern South China Sea (SSCS) are assumed to be governed by various phenomena associated with the adjacent parts of the Indian Ocean and the Pacific Ocean. We have used monthly sea level anomalies obtained from 12 tide gauge stations of PSMSL and UHSLC and merged and gridded AVISO products of SLAs (Sea Level Anomalies) derived from satellite altimeter. We find that IOD-influenced inter-annual variations are found only in the southwestern and southeastern coastal regions of SSCS. Our analysis reveals that inter-annual regional sea level drops are associated with positive phase of the IOD, and the rises with negative phase of the IOD. SLA variations at decadal scale in the southeastern and north of Gulf of Thailand correlate with Pacific Decadal Oscillations (PDO). Multiple linear regression analysis of inter-annual SLAs and climate indices shows that IOD induced inter-annual variations dominate in the southwestern SCS and it contributes to about ~40% of inter-annual sea level variation. Meanwhile, ENSO contributes to around ~30% variation in sea level in the southwestern and ~40% variation in the southeastern SSCS. The present study also suggests that inter-annual SLA variations in the SSCS can occur by ENSO and IOD induced changes in wind stress curl and volume transport variations.

**Key words:** Sea level anomalies, IOD, ENSO, southern South China Sea, wind stress curl, volume transport

## 1. Introduction

The South China Sea (SCS) is one of the western marginal seas of the Pacific Ocean, surrounded by South China, Indo China Peninsula, Malaysian Peninsula, Philippines and Borneo Island. The SCS is a semi-enclosed basin connected to the western Pacific Ocean through Taiwan Strait and Luzon Strait, Sulu Sea through Mindoro Strait and Balebec Channel, Java Sea through Gasper and Karimata Straits, and to the Indian Ocean through the Strait of Malacca. All the Straits are shallow, except the Luzon Strait, which features a sill deeper than 2000m. The maximum depth of SCS is about 4700m in the middle of the basin, but it is much shallower towards the southern part, especially in the Sunda Shelf region and in the Gulf of Thailand where depth is less than 100m. Southwestern SCS includes Gulf of Thailand, Malaysia Peninsula and Singapore Strait. Southernmost regions in the SCS encompass narrow straits and numerous small islands. Singapore Strait at the central part of the shallow Sunda shelf connects the SCS and Java Sea and part of the deep basin of the Andaman Sea.

As an Asian marginal sea, the SCS dynamics is dominated by East Asian monsoon system with north easterly winds during winter (November-February) and southwesterly winds during summer (June-August). These seasonally varying northeast (NE) and southwest (SW) monsoons induce seasonal variations in the physical characteristics in the upper ocean of SCS (Wyrтки 1961). NE monsoon winds are stronger in the SCS, with strongest winds recorded during December (Camerlengo et al., 1997). Due to these winds, an up surge of sea level is observed along the western SCS. Due to the persistence of NE monsoon winds, water tends to pile up on the western SCS (Shaw and Chao, 1994). This positive set up in sea level during winter at the southern SCS is amplified by the shallow depth of Sunda Shelf (Chen et al., 2012). Circulation in the southern SCS is relatively weak (Qu, 1999). In winter, a strong cyclonic gyre exists along the western part of the south SCS and a weaker anticyclonic circulation along the eastern part of the SCS. Circulation in the SCS is characterized by a cyclonic gyre in winter (Chu et al., 1998; Qu, 2000; Wyrтки 1961). The southward jet in winter follows throughout the western boundary, but the northward jet in summer moves away from the coast of Vietnam at about 12°N (Shaw and Chao, 1994) and there is an anticyclonic gyre in the Southern SCS and a cyclonic gyre in the northern SCS in summer (Wyrтки 1961; Fang et al., 2002; Wang et al., 2003). Overall SCS sea level is higher during summer and lower during winter (Shaw et al., 1999; Ho et al., 2000).

As the SCS is embedded between the western Pacific and the Indian Oceans, it is considerably influenced by inter-annual and decadal sea level variability associated with El Niño Southern Oscillation (ENSO) and

Pacific Decadal Oscillation (PDO) in the Pacific Ocean and Indian Ocean Dipole (IOD) in the Indian Ocean. Though ENSO is centered in the Pacific Ocean, it can influence global climate through oceanic and atmospheric teleconnections. ENSO peaks during the boreal winter while its influences on other ocean basins normally peaks 1-2 seasons later (Alexander et al., 2002). The warm phase of ENSO (El Niño) begins by a weakening of trade winds and convective activity in the equatorial western Pacific, shifts eastward leading to an altered Walker circulation with anomalous ascent over equatorial central and eastern Pacific, and descent over the SCS region. This leads to reduced convection, decrease in cloud cover and reduction in precipitation; this situation reverses during La Niña events. Hadley circulation strengthens over the eastern Pacific but weakens over the Indo-Western Pacific (Klein et al., 1999). During the cold phase (La Niña), intensified trade winds shift the warm pool farther west. This plays a significant role of SLA variation during ENSO. The strength of ENSO is measured by Southern Oscillation Index (SOI). The SOI is the surface air pressure difference between Tahiti, south Pacific islands and Darwin (Australia). El Niño episodes are associated with negative values of SOI.

SCS climate is part of the East Asian monsoon system and appears to be connected with ENSO in the Pacific (Zhang et al., 1996). There have been numerous studies describing inter-annual sea level variations in the SCS with most of the variations linked to ENSO (Hwang 2001; Fang et al., 2006; Rong et al., 2007; Zuo et al., 2012 and Peng et al., 2013) and PDO (Deng et al., 2013, Wu, 2013), and are confined to northern and eastern SCS. Rong et al. (2007) investigated different mechanisms that lead to the ENSO driven inter-annual sea level variability of SCS. Response of SCS sea level anomalies (SLAs) and sea surface temperature (SST) anomalies to ENSO are completely out of phase. ENSO induced SST variation in the SCS is believed to be through the atmospheric circulation changes. SST anomalies show double peak with relaxation between two peaks during El Niño events. A change in atmospheric circulation influences surface heat fluxes and oceanic circulation in the SCS that in turn influence the SST variation over the SCS (Wang et al., 2006). Sea level and SST have inverse responses to ENSO in SCS. But, the thermosteric Sea level anomalies, corresponding to the temperature in the intermediate layers, correlate with SOI (Rong et al., 2007).

The inter-annual relationship between the ENSO and the global climate is not stationary and can be modulated by the PDO (Mantua et al., 1997, Wu and Wang 2002). Inter-annual variability in the low latitude western Pacific has been more closely related to PDO than ENSO in recent years (Wu, 2013). The PDO is the predominant source of inter-decadal climate variability in the Pacific Northwest, defined using

the monthly anomalies of sea surface temperature (SST) in the Pacific, poleward 20°N (Mantua et al., 1997). During the positive (negative) phase of the PDO, the northwestern Pacific is characterized by negative (positive) SLAs. Geochemical studies of coral obtained from the northeastern SCS reveal the PDO activity in the SCS (Deng et al., 2013). Prominent decadal variability of SCTF is in phase with wind stress anomalies associated with PDO. The upper layer of SCTF strengthens during the positive phase of PDO (Yu et al., 2013).

Being a semi-enclosed ocean basin, SCS water can be exchanged with the surrounding ocean through the Straits. This plays an important role in sea level variations in the SCS. Intrusion of the northwest Pacific water through the Luzon Strait in the SCS is referred to as Luzon Strait transport (LST). As a direct response to the Pacific wind, Pacific origin water enters the SCS and part of the water continues southwards into the Java Sea and returns to the Pacific through the Makassar Strait (Qu et al., 2005), known as South China Sea Through Flow (SCTF). SCTF involves the inflow of cold and salty water through Luzon Strait and the outflow of warm and freshwater through the Mindoro and Karimata Straits. SCTF during ENSO increases southward flow into the Makassar Strait, inhibits tropical Pacific water injection into Makassar Strait, thereby reduces Indonesian through Flow (ITF) into the Indian Ocean (Gordon et al., 2012). Most of the water entering the SCS circulates along the western boundary of SCS and exits through Karimata Strait. Water exchange between SCS and Pacific Ocean is mostly concentrated in the upper 300m (Shaw and Chao, 1994). The LST carries the ENSO signals into the SCS. Water enters the SCS with a low temperature through LST and leaves with a higher temperature through Karimata and Mindoro Straits. Increased LST during El Niño produces a stronger than normal cooling advection, which eventually cools SCS and leads to negative SLAs (Qu et al., 2004). SCTF plays an important role in the climate variability of Indo-Pacific Ocean by changing the upper ocean thermal structure. Decadal variability was identified as the dominant mode of upper ocean heat content (Song et al., 2014). Wind stress variations in the western Pacific plays a major role in the inter-annual and decadal variability of SCTF (Wang et al., 2006 and Liu et al., 2010).

SCS summer monsoon is influenced by IOD through its impacts on atmospheric circulations (Yuan et al., 2008). The IOD is the coupled ocean and atmosphere phenomena in the equatorial Indian Ocean that evolves a positive mode (PIOD) and negative mode (NIOD) in which western Indian Ocean becomes alternatively warmer and colder than eastern Indian Ocean (Saji et al., 1999). The positive IOD events generally occur during El Niño and negative IOD with La Niña events, but they can occur independently

(Yamagata et al., 2004). IOD shows a quasi-biennial variation due to the sequential existence of NIOD followed by a PIOD (Saji et al., 1999; Rao et al., 2002; Behera et al., 2003; Feng and Meyers, 2003). Dipole Mode Index (DMI), proxy for IOD is the difference between sea surface temperature (SST) in the western (50°E -70°E, 10°S -10°N) and eastern (90°E -110°E, 10°S - 0°S) equatorial Indian Ocean (Saji et al., 1999).

In the present study, satellite altimetry SLA data for the last two decades, as well as tide gauge records at 12 locations are employed to examine the inter-annual sea level variations in the Southern SCS.

## **2. Data**

Monthly sea level anomalies were obtained from Permanent Service for Mean Sea Level (PSMSL) and University of Hawaii Sea Level Centre (UHSLC). Figure 1 shows locations of tide gauge stations. Details of sea level stations and data duration are given in Table 1. Merged and gridded products of MSLA (Maps of Sea Level Anomaly), derived from satellite altimeter, are obtained from <https://www.aviso.oceanobs.com>. This MSLA is produced by AVISO (Archiving, Validation, and Interpretation of Satellite Oceanographic data), based on TOPEX/Poseidon, Jason 1, ERS-1 and 2 altimeter observations. In this study, we have averaged the sea level anomaly data available at weekly intervals to obtain monthly mean sea level anomalies for 1993-2011.

In this study, we characterize the main climate modes that drive the inter-annual sea level variation over the SCS, by analyzing the correlation between SOI (Southern Oscillation Index), DMI (Dipole mode index) and PDO (Pacific Decadal Oscillation) index. The ENSO index (SOI) is downloaded from <http://www.cpc.ncep.noaa.gov/data/indices/> and DMI defined by Saji et al. (1999) is downloaded from [http://www.jamstec.go.jp/frcgc/research/d1/iod/e/iod/dipolemode\\_index.html](http://www.jamstec.go.jp/frcgc/research/d1/iod/e/iod/dipolemode_index.html). PDO, based on north Pacific SST variations, are obtained from <http://jisao.washington.edu/pdo/PDO.latest>. Classification of IOD events into positive and negative and warm and cold phases of ENSO into El Nino and La Nina years (Table 2) is done based on available literature information.

Volume transport between SCS and adjacent oceans is estimated based on SODA (Simple Ocean Data Assimilation) global reanalysis datasets. These datasets are provided on 0.5° x 0.5° horizontal resolution with 40 levels from 5m to 5347m depth range for the period 1958 to 2008. Zonal and meridian velocities are used to calculate the volume transport in the upper 300m. ERA-Interim reanalysis surface wind products with 1.5° resolution are downloaded from <http://data-portal.ecmwf.int/data/>.

### 3. Methodology

In order to study the relationship between the sea level variation in SCS and climatic modes at inter-annual time scale, the observed monthly sea level data series were subtracted from mean to obtain Sea Level Anomalies (SLA). SLAs are mainly dominated by inter-annual and inter decadal fluctuations. Seasonal signals in the monthly SLAs are large and appropriate filtering is needed for visualization of interannual signals. In the present study, seasonal and annual signals were first removed. A Butterworth low-pass filter of order 5 with cut off frequency of 1.5years was applied to extract inter-annual signals. Cross-correlation between inter-annual SLAs and climate indices was carried out to understand the lead and lag of the climate events. Wavelet analysis (Torrence and Compo, 1998) of SLAs was performed to characterize the temporal variation of inter-annual signals.

In this study, the volume transport is estimated based on SODA global analysis zonal and meridional velocity components. Meridional volume transport for the upper 300m is estimated over the region 106E-110E, 4N-8N. The horizontal transport of volume ( $H_v$ ) across any ocean basin of width  $L$  and depth  $h(x)$  is defined as,

$$H_v(t) = \int_0^L \int_{-h(x)}^0 V(x, z, t) dz dx$$

where,  $V(x, z, t)$  is the velocity component.

Empirical orthogonal Function (EOF) analysis was performed to describe spatial and temporal behavior of SLAs (Preisendorfer, 1988). EOF analysis has been carried out on the gridded monthly sea level anomalies for the period 1993-2012. Each EOF mode consists of a spatial pattern modulated by an associated time series. The first few EOF modes represent the majority of variance in a data series. In the present study, four leading EOFs explain 82% of total variance. Spectral and wavelet analyses of the temporal functions were carried out to investigate the temporal variability of a given EOF mode that can identify the frequencies of the processes contributing to this mode. Correlation between temporal functions and major climate indices were performed to quantify the role of external forcing on each EOF. A multi-linear regression model of sea level as a dependent parameter and climate indices as independent parameters, has been established to quantify the influence of each parameter on Inter-annual sea level variability.

### 4. Results and Discussions

#### *4.1. Sea level inter-annual variability and its relation to major climate indices*

In this study we explore the inter-annual sea level variations and their relation to various climate modes. We find that SLA has least correlation with SOI along the southwestern region of SCS (represented by SLAs at Sembawang and Tanjong Pagar in the Singapore Strait (Fig. 2)). However, SLAs in the Sultan Shoal and Raffles Lighthouse are strongly correlated with ENSO, with correlation coefficient of 0.65 at 3 month lag time (Fig. 2 a&d). Multiple linear regression analysis shows that 21.5% of variability is accounted for by ENSO in the Sultan Shoal and 38% in the Raffles Lighthouse. Sea level along Borneo Island negatively corresponds to ENSO and positively to IOD indices (Fig. 3). All these stations show maximum correlation of 0.75 at 2 month lag time. ENSO accounts for 52.4% of inter-annual sea level variations at Kota Kinabalu, 45% at Kudat, 41% at Luban and 12% at Peurto Princessa. Inter-annual SLAs in the northwestern stations including Gulf of Thailand, east coast of Vietnam, are least correlated to SOI (Fig. 4 a.1-d.1). SLA at Getting along the east coast of Malay Peninsula is correlated to SOI and explains 36% of inter-annual sea level variability. Ko Lak along the head of the Gulf of Thailand is least correlated with all the climate indices. These results show that SLA and SOI vary coherently along the southwestern and southeastern regions of SCS, but to a lesser degree on the northwest. The inter-annual sea level drops are associated with El Nino and rises associated with La Nina.

In order to extract the sea level variability associated with IOD, we have used IOD index as defined by Saji et al. (1999). Recent analysis of Luu et al. (2014) showed that IOD modulates sea level anomalies in the Malacca strait in the range of  $\pm 2$  cm. During Positive IOD events, negative SLAs were observed along the southwest coast of SSCS (Fig. 2 a.2-d.2). Along SS and Malay Peninsula, SLAs strongly correlated with DMI negatively at 1month lag. The Gulf of Thailand and northern SCS SLAs are not correlated with DMI (Fig. 4 a.2-d.2). Sea level anomalies along the southeastern SCS show strong negative correlation with IOD at 2 month lag time (Fig. 3, a.2-d.2). IOD contributes to an average of 40 % of inter-annual sea level variations in the Singapore Strait (Sultan Shoal and Raffles Lighthouse) and 20% along the southeast region. Regression analysis shows that northwest SCS, that is, north of Malay Peninsula, is not influenced by IOD.

In order to assess the contribution of ENSO and IOD events, as independent variables, to the interannual SLAs, we used the partial correlation technique. The results of spatial distribution of partial correlation between SOI and SLAs indicate significant impact of ENSO on southeastern and southwestern coastal boundaries of SCS (Fig. 5 a). ENSO related coastal Kelvin wave propagation into the southeastern SCS

through the Mindoro Strait induces negative (positive) SLAs in the southeastern SCS during El Nino (La Nina) event (Liu et al., 2011). Good correlation is found between IOD and SLAs in the Malacca Strait and Singapore Strait, and correlation weakens in the rest of SCS (Fig. 5 b). Partial correlation of tide gauge SLAs in the southeastern SCS shows  $\sim 0.65$  correlation with ENSO and  $\sim -0.30$  with IOD. Singapore Strait SLAs show a correlation of  $\sim 0.5$  with IOD and ENSO.

As SCS is one of the marginal seas of Western Pacific, it is considerably influenced by SST oscillations (PDO) in the North Pacific Ocean. Inter annual and longer term sea level variability in eastern SCS is negatively correlated with PDO (Han et al., 2008). Our analysis shows that SLAs in the southeastern and northwestern SCS are negatively correlated to PDO (Fig. 5 and Fig. 6). In the southeastern SCS, 30% of sea level variability is accounted for by PDO. SLA is only 4% of inter-annual sea level variations at Singapore Strait, and hence not influenced by PDO.

Spatial correlation pattern of SODA sea surface height anomalies during the period 1975 to 2010, with PDO show strong negative correlation along the southeastern and northwestern SCS (Fig. 7). SODA version 2.2.4 data is potentially a useful tool to examine ocean decadal climate variability across the Indo-Pacific Ocean (Vargas et al., 2014). Our analysis shows that the estimated Luzon Strait transport and Mindoro Strait transport correlate with ENSO (correlation coefficient  $\sim 0.5$ ), but, not with PDO (correlation coefficient  $< 0.2$ ). Also we find that the decadal variations in the SCTF is not in phase with PDO. Wavelet analysis of SLA was performed after eliminating seasonal signals. SLAs show significant decadal and inter annual signals (Fig. 8). Significant inter annual variations in SLAs at 2-4 year cycles associated with IOD and 4-8 year periods associated with ENSO are seen southwest and southeast of SCS (Fig. 8, 1&2). SLAs in Ko Lak do not show any significant inter annual signal; north of Gulf of Thailand shows decadal signals in SLAs.

#### *4.2. Empirical orthogonal function (EOF) decomposition*

To analyze the characteristics of SCS inter-annual sea level variability, EOF decomposition of altimetry SLA was performed over the period 1993-2012. Fig. 9.1 (a & b) shows second and third modes of EOF decomposition, respectively. First mode accounts for seasonal sea level variation, which contributes to 41% of total variance. Spatial variation of second mode EOF is shown in Figure 9.1 (a). Low SLAs are observed along the southwestern region. Principal component of EOF2 correlates with SOI with correlation coefficient of 0.84 (Figure 9.2 (a)), which accounts for 26% of total variance. EOF3 which represents spatial variation due to IOD is not uniform in the SCS (Figure 9.1 (b)), which accounts for 9%



of total variance. Principal component of EOF3 is correlated with DMI (Figure 9.2 (b)). Southwest coast of Sumatra shows negative SLAs and inside the SCS basin shows positive SLAs, except along the southwestern coastal region. EOF4 represents decadal variations of sea level, which accounts for 2.7% of total variance.

EOF decomposition of wind stress curl calculated from ERA/Interim surface wind in the SCS shows strong inter annual variability in accordance with the climate indices. Principal component of EOF2 along with SOI shows that positive (negative) wind stress curl leads to negative (positive) sea level anomalies during El Nino (La Nina) events (Fig. 10.1). Correlation of SOI with EOF 2 is -0.65. Spatially uniform southwesterly wind anomaly is found over the SCS during positive IOD events (Saji et al., 1999). These southerly wind anomalies lead to anticyclonic circulation in the SCS, and thus to higher SLAs except for the coastal regions in the southwest and south east. Principal component of EOF 4 of wind stress curl is strongly negatively correlated to DMI (-0.72). Negative wind stress curl is found in SCS during strong PIOD events (Figure 10.2).

#### *4.3. Inter-annual variation of volume transport in the SCS*

Since SCS is a semi-enclosed ocean basin, sea water can exchange with surrounding oceans through a few straits that play an important role in the sea level variations in the SCS. South China Sea through Flow (SCTF), which is the SCS branch of ITF, is an important passage for Pacific water flow into the Indian Ocean (Fang et al., 2002). Pacific water enters the SCS through the Luzon Strait and most of the water will circulate along the western boundary of SCS and exit through Karimata Strait on the south, which connects SCS to Java Sea (Qu, 2005). One part of this outflow may return to the Pacific through Makassar Strait. Annual cycles of volume transport show maximum during January (3.5 Sv southward) and minimum during August (1.5 Sv northward). Estimated net volume transport strongly corresponds to sea level anomalies in the above mentioned region at inter annual scale (Figure 11), with a correlation coefficient of -0.8. Here, negative values correspond to southward and positive values correspond to northward volume transport. When southward volume transport increases (decreases) SLA also increases (decreases). During typical El Nino events of 1987, 1991, 1997 and 2002, net volume transport became northward, and the pattern reverses during the La Nina events of 1988,1998,1999,2000 and 2005 (Figure 12).

## **5. Conclusions**

Sea level variations in the southern SCS were investigated using tide gauge as well as altimetry data. Sea levels vary at significant inter annual scales. Prominent variations occurred along southwestern and southeastern coastal regions. Inter annual variations are modulated by ENSO significantly. IOD-influenced inter annual variations are found only along the coastlines of Singapore Strait and southeastern coastal regions. SLA shows a correlation of 0.65 at 3 month lag time with SOI, and a correlation of -0.60 at 1 month lag with DMI in the Singapore Strait region. SLAs along southeastern SCS is also correlated with ENSO and IOD. SLA shows correlation of 0.75 with SOI and (-0.5) with DMI at 2 month lag time. PDO influences interannual sea level variations along southeast regions and regions north of Gulf of Thailand (correlation -0.5). Multiple linear regression analysis of inter annual SLAs with these climate indices quantifies influence of each climate mode on sea level.

At inter annual scale, sea level variations are influenced by wind stress curl and volume transport. Positive (negative) wind stress curl during El Nino (La Nina) leads to negative (positive) sea level anomalies. During a PIOD event, southern SCS region is characterized by southerly winds, and the resulting anticyclonic circulation leads to basin wide positive sea level anomalies except for the coastal locations along the southwest and southeast of SCS. Volume transport calculated over a region in the southern SCS shows strong Interannual variability with ENSO, which leads to ENSO induced inter annual sea level variations.

## 6. Acknowledgements

We thank Directors of CSIR-NIO, Goa and TMSI, NUS for providing the facilities. Monthly tide gauge sea level data has been obtained from the Permanent service for mean sea level (PSMSL) and University of Hawaii Sea Level Centre (UHSLC). The ENSO index (SOI) is downloaded from <http://www.cpc.ncep.noaa.gov/data/indices/>. DMI is downloaded from [http://www.jamstec.go.jp/frcgc/research/d1/iod/e/iod/dipolemode\\_index.html](http://www.jamstec.go.jp/frcgc/research/d1/iod/e/iod/dipolemode_index.html). PDO index is obtained from <http://jisao.washington.edu/pdo/PDO.latest>. ERA-Interim reanalysis surface wind products are obtained from <http://data-portal.ecmwf.int/data/>. This is NIO contribution no. xxxx.

## 7. References

Alexander, M.A., Bladé, I., Newman, M., Lanzante, J.R., Lau, N.-C. and Scott, J.D., 2002. The Atmospheric Bridge: The Influence of ENSO Teleconnections on Air–Sea Interaction over the Global Oceans. *Journal of Climate*, 15(16).

- Behera, S.K. and Yamagata, T., 2003. Influence of Indian Ocean dipole on southern oscillation. *Journal of the Meteorological Society of Japan*, 81(1): 169-177.
- Camerlengo, A. and Demmler, M.I., 1997. Wind-driven circulation of peninsular Malaysia's eastern continental shelf. *Scientia Marina*, 61: 203-211.
- Chen, H., Tkalich, P., Malanotte-Rizzoli, P. and Wei, J., 2012. The forced and free response of the South China Sea to the large-scale monsoon system. *Ocean Dynamics*, 62(3): 377-393.
- Chu, P.C., Edmons, N.L. and Fan, C., 1999. Dynamical mechanisms for the South China Sea seasonal circulation and thermohaline variabilities. *Journal of Physical Oceanography*, 29(11): 2971-2989.
- Deng, W., Wei, G., Xie, L., Ke, T., Wang, Z., Zeng, T. and Liu, Y., 2013. Variations in the Pacific Decadal Oscillation since 1853 in a coral record from the northern South China Sea. *Journal of Geophysical Research: Oceans*, 118(5): 2358-2366.
- Emery, W.J. and Thomson, R.E., 2001. *Data analysis methods in physical oceanography*. Elsevier.
- Fang, G., Chen, H., Wei, Z., Wang, Y., Wang, X. and Li, C., 2006. Trends and interannual variability of the South China Sea surface winds, surface height, and surface temperature in the recent decade. *Journal of Geophysical Research: Oceans (1978–2012)*, 111(C11).
- Fang, W., Fang, G., Shi, P., Huang, Q. and Xie, Q., 2002. Seasonal structures of upper layer circulation in the southern South China Sea from in situ observations. *Journal of Geophysical Research: Oceans (1978–2012)*, 107(C11): 23-1-23-12.
- Feng, M. and Meyers, G., 2003. Interannual variability in the tropical Indian Ocean: a two-year time-scale of Indian Ocean Dipole. *Deep Sea Research Part II: Topical Studies in Oceanography*, 50(12): 2263-2284.
- Gordon, A.L., Huber, B.A., Metzger, E.J., Susanto, R.D., Hurlburt, H.E. and Adi, T.R., 2012. South China Sea through flow impact on the Indonesian through flow. *Geophysical Research Letters*, 39(11).
- Han, G. and Huang, W., 2008. Pacific Decadal Oscillation and Sea Level Variability in the Bohai, Yellow, and East China Seas. *Journal of Physical Oceanography*, 38(12).
- Ho, C.R., Zheng, Q., Soong, Y.S., Kuo, N.J. and Hu, J.H., 2000. Seasonal variability of sea surface height in the South China Sea observed with TOPEX/Poseidon altimeter data. *Journal of Geophysical Research: Oceans (1978–2012)*, 105(C6): 13981-13990.
- Hwang, C. and Chen, S.A., 2000. Circulations and eddies over the South China Sea derived from TOPEX/Poseidon altimetry. *Journal of Geophysical Research: Oceans (1978–2012)*, 105(C10): 23943-23965.
- Hwang, C. and Chen, S.A., 2000. Fourier and wavelet analyses of TOPEX/Poseidon-derived sea level anomaly over the South China Sea: A contribution to the South China Sea Monsoon Experiment. *Journal of Geophysical Research: Oceans (1978–2012)*, 105(C12): 28785-28804.
- Hwang, C., 2001. Interannual variation of sea level of South China Sea and its relationship with ENSO, ASPG Fourth Workshop, ASPG Management board and the Shanghai Astronomical Observatory, CAS, Shanghai, PR China, pp. 14-19.

- Klein, S.A., Soden, B.J. and Lao, N.-C., 1999. Remote sea surface temperature variations during ENSO: Evidence for a tropical atmospheric bridge. *Journal of Climate*, 12(4).
- Liu, Q., Wang, D., Zhou, W., Xie, Q., Zhang, Y., 2010. Covariation of the Indonesian throughflow and South China Sea throughflow associated with the 1976/77 regime shift. *Advances in Atmospheric Sciences* 27, 87-94.
- Liu, Q., Feng, M., Wang, D., 2011. ENSO-induced interannual variability in the southeastern South China Sea. *Journal of oceanography* 67, 127-133.
- Liu, X., Liu, Y., Guo, L., Rong, Z., Gu, Y. and Liu, Y., 2010. Interannual changes of sea level in the two regions of East China Sea and different responses to ENSO. *Global and Planetary Change*, 72(3): 215-226.
- Mantua, N.J., Hare, S.R., Zhang, Y., Wallace, J.M. and Francis, R.C., 1997. A Pacific interdecadal climate oscillation with impacts on salmon production. *Bulletin of the American Meteorological Society*, 78(6): 1069-1079.
- Peng, D., Palanisamy, H., Cazenave, A. and Meyssignac, B., 2013. Interannual Sea Level Variations in the South China Sea Over 1950–2009. *Marine Geodesy*, 36(2): 164-182.
- Preisendorfer, R.W. and Mobley, C.D., 1988. *Principal component analysis in meteorology and oceanography*, 17. Elsevier Science Ltd.
- Qu, T., Kim, Y.Y., Yaremchuk, M., Tozuka, T., Ishida, A. and Yamagata, T., 2004. Can Luzon Strait transport play a role in conveying the impact of ENSO to the South China Sea? *Journal of Climate*, 17(18).
- Qu, T., Mitsudera, H. and Yamagata, T., 1999. A Climatology of the Circulation and Water Mass Distribution near the Philippine Coast\*. *Journal of Physical Oceanography*, 29(7): 1488-1505.
- Qu, T., Mitsudera, H. and Yamagata, T., 2000. Intrusion of the North Pacific waters into the South China Sea. *Journal of Geophysical Research: Oceans* (1978–2012), 105(C3): 6415-6424.
- Rao, S.A., Behera, S.K., Masumoto, Y. and Yamagata, T., 2002. Interannual subsurface variability in the tropical Indian Ocean with a special emphasis on the Indian Ocean dipole. *Deep Sea Research Part II: Topical Studies in Oceanography*, 49(7): 1549-1572.
- Rong, Z., Liu, Y., Zong, H. and Cheng, Y., 2007. Interannual sea level variability in the South China Sea and its response to ENSO. *Global and Planetary Change*, 55(4): 257-272.
- Saji, N., Goswami, B.N., Vinayachandran, P. and Yamagata, T., 1999. A dipole mode in the tropical Indian Ocean. *Nature*, 401(6751): 360-363.
- Shaw, P.-T. and Chao, S.-Y., 1994. Surface circulation in the South China Sea. *Deep Sea Research Part I: Oceanographic Research Papers*, 41(11): 1663-1683.
- Shaw, P.-T., Chao, S.-Y. and Fu, L.-L., 1999. Sea surface height variations in the South China Sea from satellite altimetry. *Oceanologica Acta*, 22(1): 1-17.

- Song, W., Lan, J., Liu, Q., Sui, D., Zeng, L., Wang, D., 2014. Decadal variability of heat content in the South China Sea inferred from observation data and an ocean data assimilation product. *Ocean Sci.*, 10, 135–139.
- Tkalich, P., Vethamony, P., Luu, Q.-H. and Babu, M., 2013. Sea level trend and variability in the Singapore Strait. *Ocean Science*, 9(2).
- Torrence, C. and Compo, G.P., 1998. A practical guide to wavelet analysis. *Bulletin of the American Meteorological Society*, 79(1): 61-78.
- Vargas-Hernandez, J.M., Wijffels, S., Meyers, G., Holbrook, N.J. , 2014. Evaluating SODA for Indo-Pacific Ocean decadal climate variability studies. *Journal of Geophysical Research: Oceans* 119, 7854-7868.
- Wang, C., Wang, W., Wang, D. and Wang, Q., 2006. Interannual variability of the South China Sea associated with El Niño. *Journal of Geophysical Research: Oceans (1978–2012)*, 111(C3).
- Wang, D., Liu, Q., Huang, R.X., Du, Y. and Qu, T., 2006. Interannual variability of the South China Sea throughflow inferred from wind data and an ocean data assimilation product. *Geophysical research letters*, 33(14).
- Wang, G., Su, J. and Chu, P.C., 2003. Mesoscale eddies in the South China Sea observed with altimeter data. *Geophysical Research Letters*, 30(21).
- Wu, C.-R., 2013. Interannual modulation of the Pacific Decadal Oscillation (PDO) on the low-latitude western North Pacific. *Progress in Oceanography*, 110: 49-58.
- Wu, R. and Wang, B., 2002. A Contrast of the East Asian Summer Monsoon–ENSO Relationship between 1962–77 and 1978–93. *Journal of Climate*, 15(22).
- Wyrtki, K., 1961. *Physical oceanography of the southeast Asian waters*.
- Yamagata, T., Behera, S.K., Luo, J.J., Masson, S., Jury, M.R. and Rao, S.A., 2004. Coupled ocean-atmosphere variability in the tropical Indian Ocean. *Earth's Climate*: 189-211.
- Yu, K. and Qu, T., 2013. Imprint of the Pacific Decadal Oscillation on the South China Sea Throughflow Variability. *Journal of Climate*, 26(24).
- Zhang, Y., Sperber, K., Boyle, J., Dix, M., Ferranti, L., Kitoh, A., Lau, K., Miyakoda, K., Randall, D. and Takacs, L., 1997. East Asian winter monsoon: results from eight AMIP models. *Climate dynamics*, 13(11): 797-820.
- Zhou, J., Li, P. and Yu, H., 2012. Characteristics and mechanisms of sea surface height in the South China Sea. *Global and Planetary Change*, 88: 20-31.

Table 1. Tide gauge data from the SCS used in the present study

Name	Lon (°E)	Lat (°N)	Data duration	Span (years)
------	----------	----------	---------------	--------------

Qui Nhon	109.25	13.767	1980-2006	27
Vung Tau	107.067	10.33	1980-2001	22
Ko Lak	99.817	11.8	1980-2011	32
Geting	102.1	6.23	1987-2011	25
Raffles	103.733	1.5	1980-2011	32
Tanjong Pagar	103.85	1.25	1989-2011	23
Sultan shoal	103.633	1.233	1980-2011	32
Sembawang	103.833	1.45	1980-2011	32
Luban	115.25	5.273	1996-2011	16
Kota Kinabalu	116.067	5.983	1988-2011	22
Kudat	116.844	6.879	1996-2011	16
Peurto Princesa	118.733	9.75	1991-2011	21

Table 2. Years of ENSO and IOD events (\* indicates strong events)

El Nino years 1965*,1968,1972*,1976,1982*,1986,1987,1991*, 1994, 1997*,2002,2004,2006,2009	La Nina Years 1964,1970,1973*,1975*,1983,1988*,1995, 1998, 1999*,2000,2005,2007,2010*,2011
Positive IOD years 1961,1963*,1967,1972*,1976*,1983,1982*, 1987*,1997*,2003,2006*,2007,2008,2012	Negative IOD years 1958,1960,1964*,1971*,1989*,1992,1996, 1998*, 2001, 2005, 2010.

## List of figures

Fig. 1. Area of study (SCS). Depth contours of deep water region are based on ETOPO2 data sets. Black circles represent tide gauge locations.

Fig. 2. Relation between inter-annual SLAs in the Singapore Strait and SOI (left) and DMI (right).

[a] Sembawang, [b] Sultan Shoal, [c] Tanjong Pagar and [d] Raffles Lighthouse.

Fig. 3. Relation between inter-annual SLAs along the southeast SCS and SOI (left), and DMI (right). [a] Luban, [b] Kota Kinabalu, [c] Kudat and [d] Peurto Princesa.

Fig. 4. Relation between inter-annual SLAs along the northwest of SCS and SOI (left) and DMI (right). [a] Geting, [b] Ko Lak, [c] Vung Tau and [d] Qui Nhon.

Fig. 5. Spatial distribution of partial correlation pattern of inter-annual SLA with SOI (a) and DMI (b).

Fig. 6. Relation between inter-annual SLAs along the southeast (left panel) and northwest (right panel) SCS and PDO index. [a.1] Luban, [b.1] Kota Kinabalu, [c.1] Kudat, [d.1] Peurto Princesa, [a.2] Getting, [b.2] Ko Lak, [c.2] Vung Tau, [d.2] Qui Nhon.

Fig. 7. Spatial correlation pattern of inter-annual sea surface height anomalies (1975 – 2010) with PDO index.

Fig. 8. Wavelet plots of inter-annual sea level anomalies (i) southwest - [a] Sembawang, [b] Sultan Shoal, [c] Tanjong Pagar and [d] Raffles Lighthouse, (ii) southeast- [a] Luban, [b] Kota Kinabalu, [c] Kudat and [d] Peurto Princesa, and (iii) northwest- [a] Geting, [b] Ko Lak, [c] Vung Tau, [d] Qui Nhon

Fig. 9.1. Spatial patterns of EOF, [a] EOF2 and [b] EOF3.

Fig. 9.2. EOF principal components of SLA compared with SOI [a] and DMI [b].

Fig. 10.1. EOF principal component of wind stress curl compared with SOI

Fig. 10.2. EOF principal component of wind stress curl compared with DMI

Fig. 11. SLA is compared with SCTF volume transport.

Fig. 12. SCTF volume transport is compared with SOI.

Fig. 1. Area of study (SCS). Depth contours of deep water region are based on ETOPO2 data sets. Black circles represent tide gauge locations.

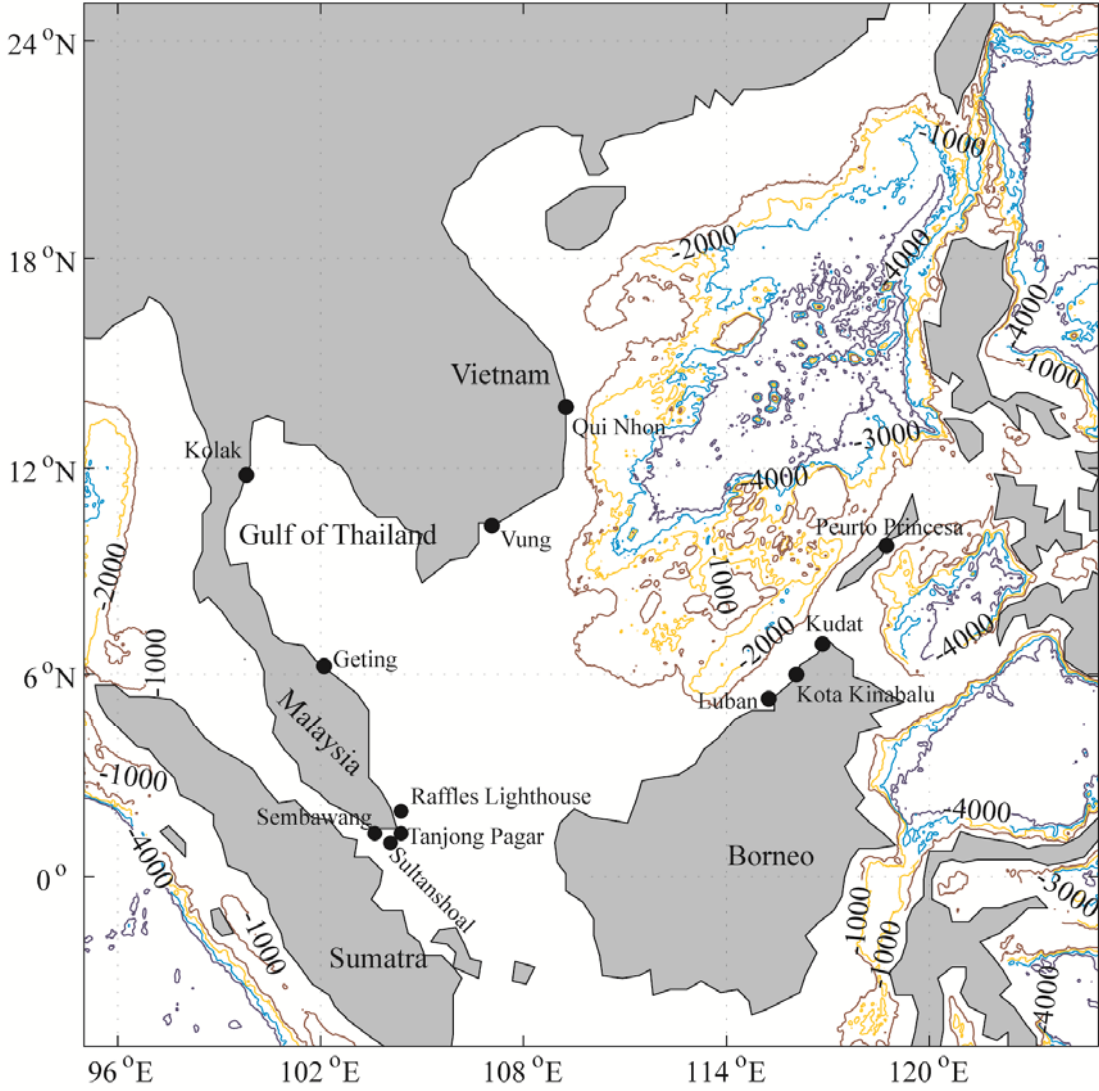




Fig. 2. Relation between inter-annual SLAs in the Singapore Strait and SOI (left) and DMI (right). [a] Sembawang, [b] Sultan Shoal, [c] Tanjong Pagar and [d] Raffles Lighthouse.

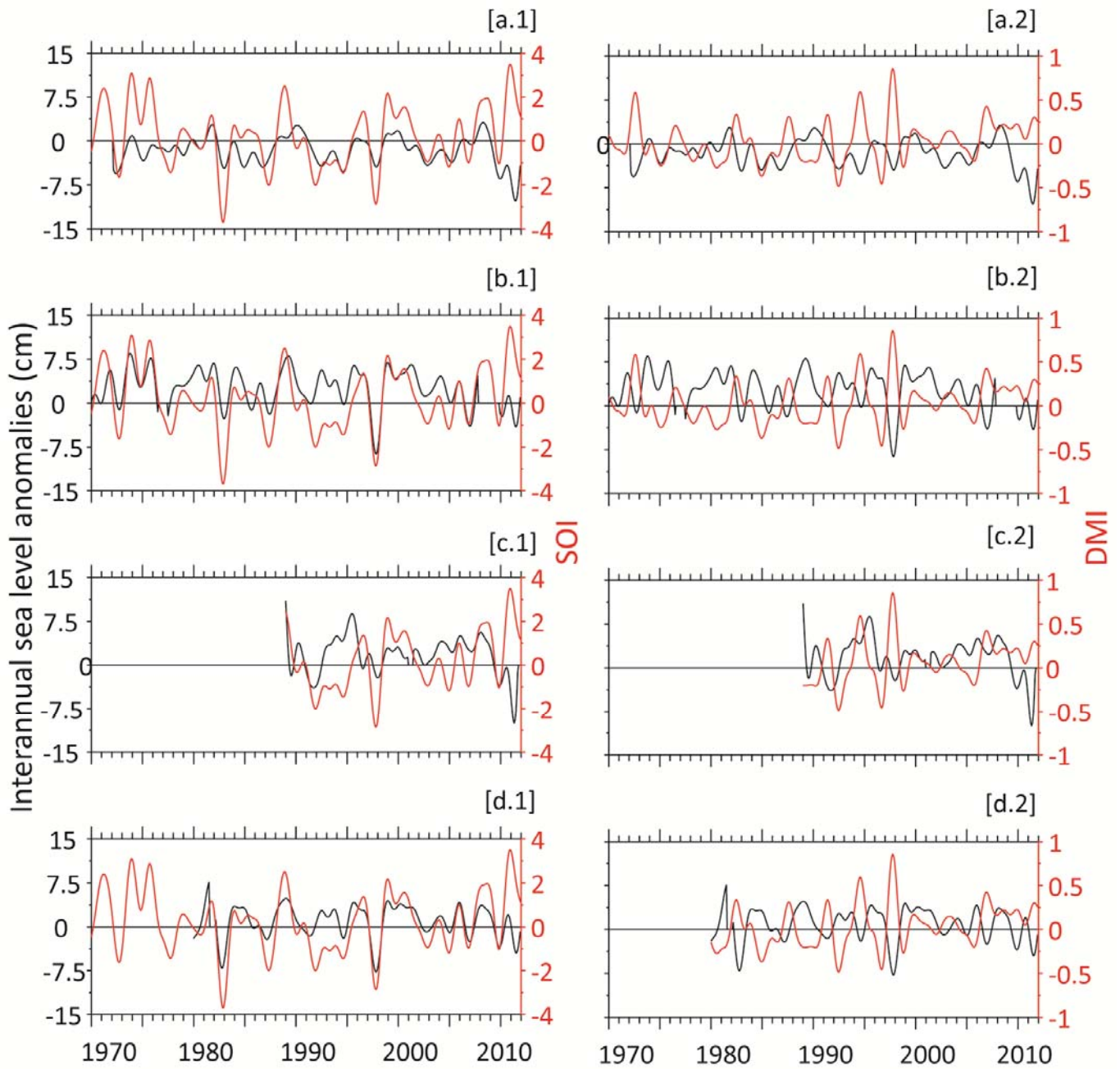


Fig. 3. Relation between inter-annual SLAs along the southeast SCS and SOI (left), and DMI (right). [a] Luban, [b] Kota Kinabalu, [c] Kudat and [d] Peurto Princesa.

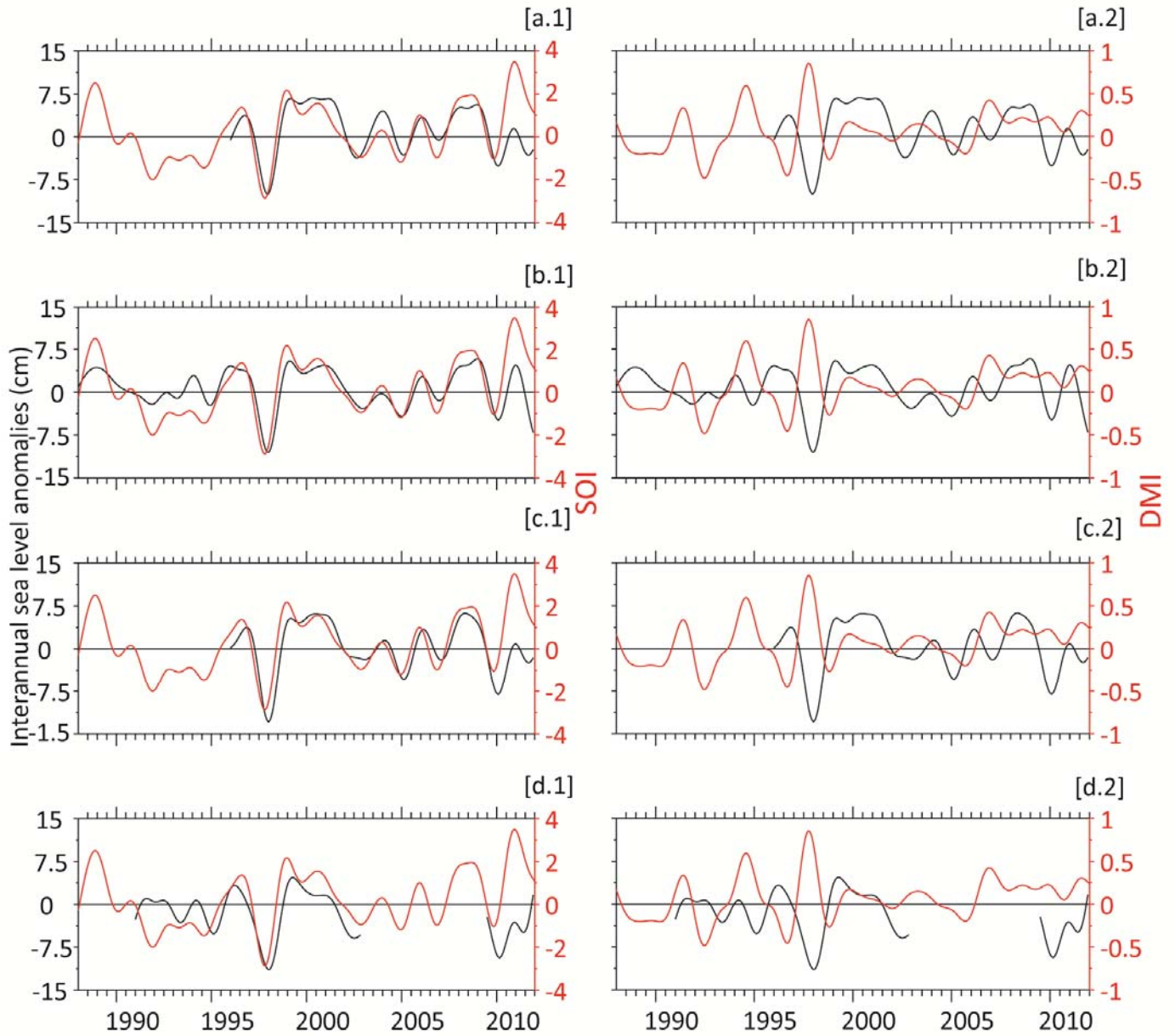


Fig. 4. Relation between inter-annual SLAs along the northwest of SCS and SOI (left) and DMI (right). [a] Geting, [b] Ko Lak, [c] Vung Tau and [d] Qui Nhon.

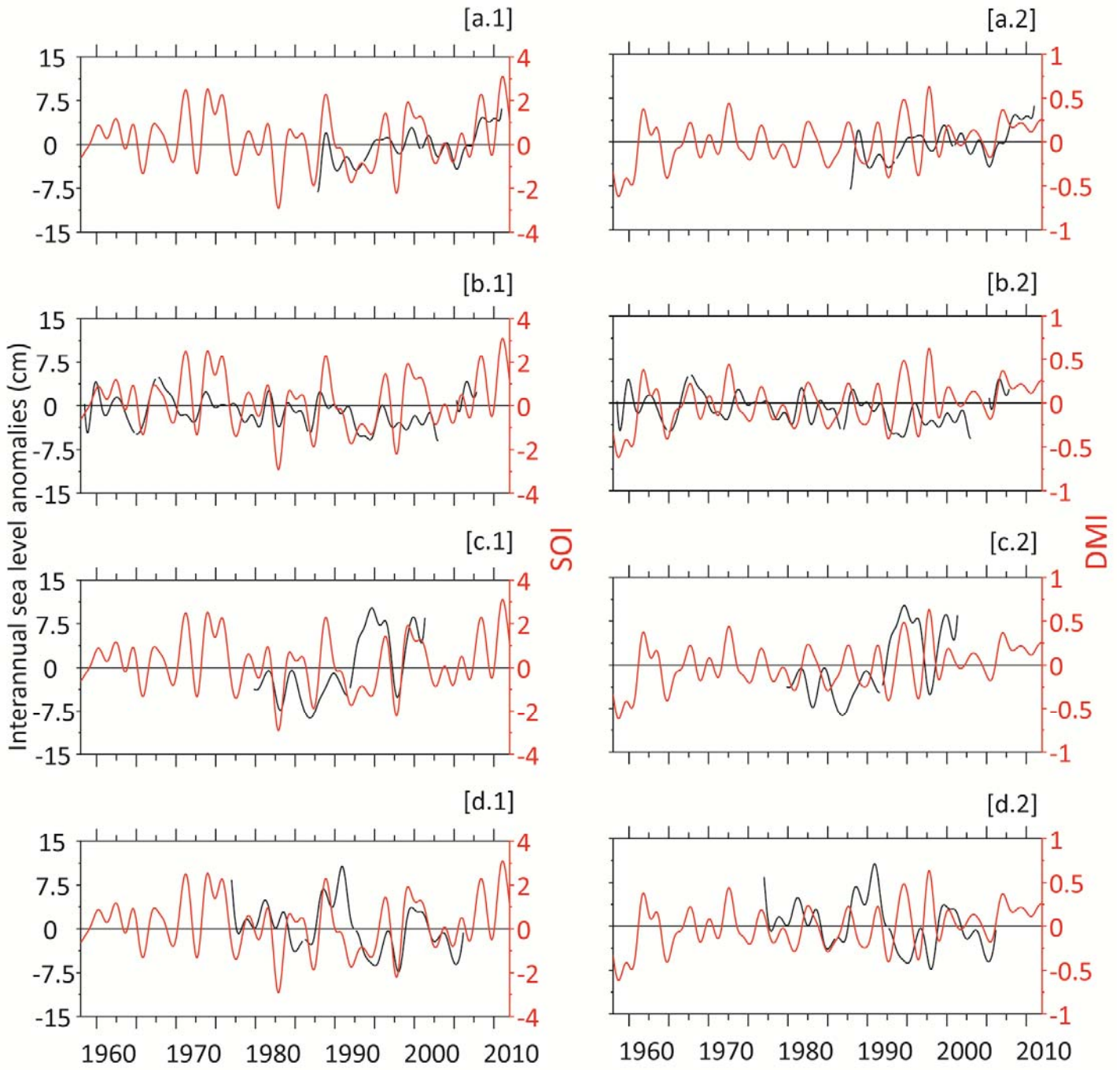


Fig. 5. Spatial distribution of partial correlation pattern of inter-annual SLA with SOI (a) and DMI (b).

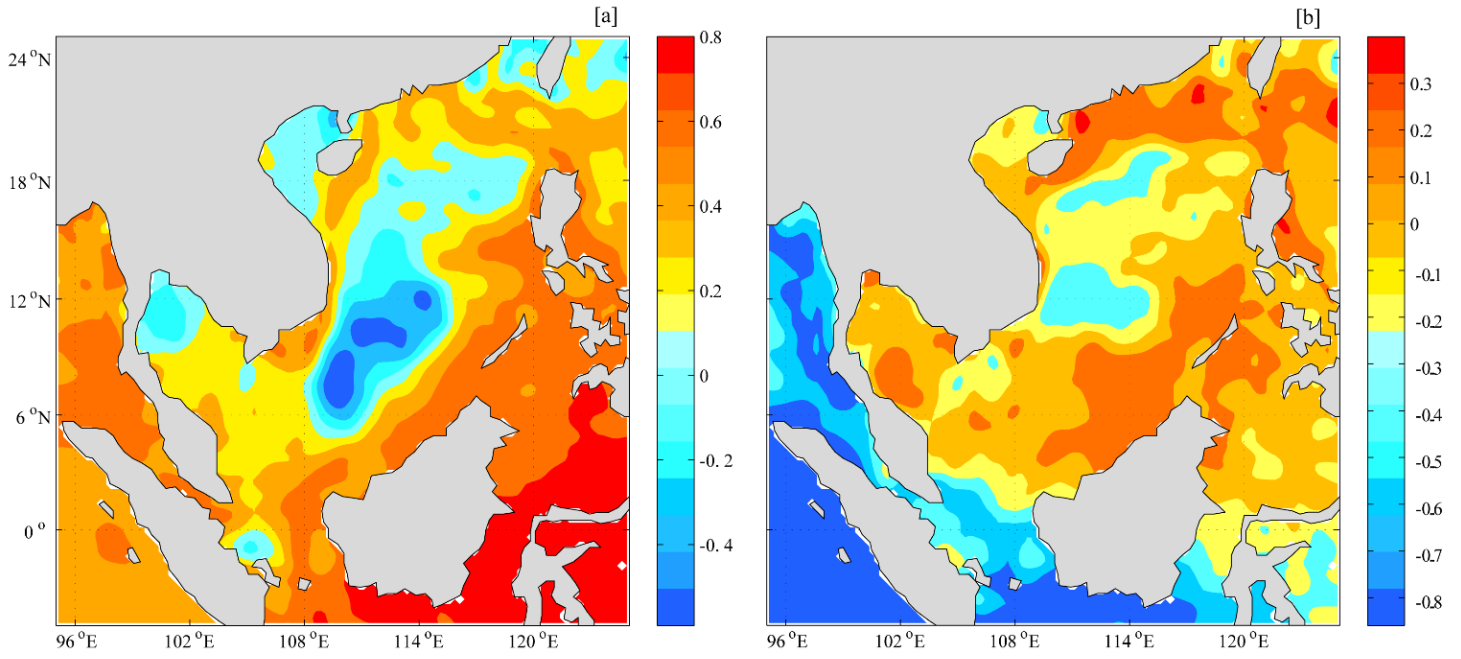


Fig. 6. Relation between inter-annual SLAs along the southeast (left panel) and northwest (right panel) SCS and PDO index. [a.1] Luban, [b.1] Kota Kinabalu, [c.1] Kudat, [d.1] Peurto Princesa, [a.2] Getting, [b.2] Ko Lak, [c.2] Vung Tau, [d.2] Qui Nhon.

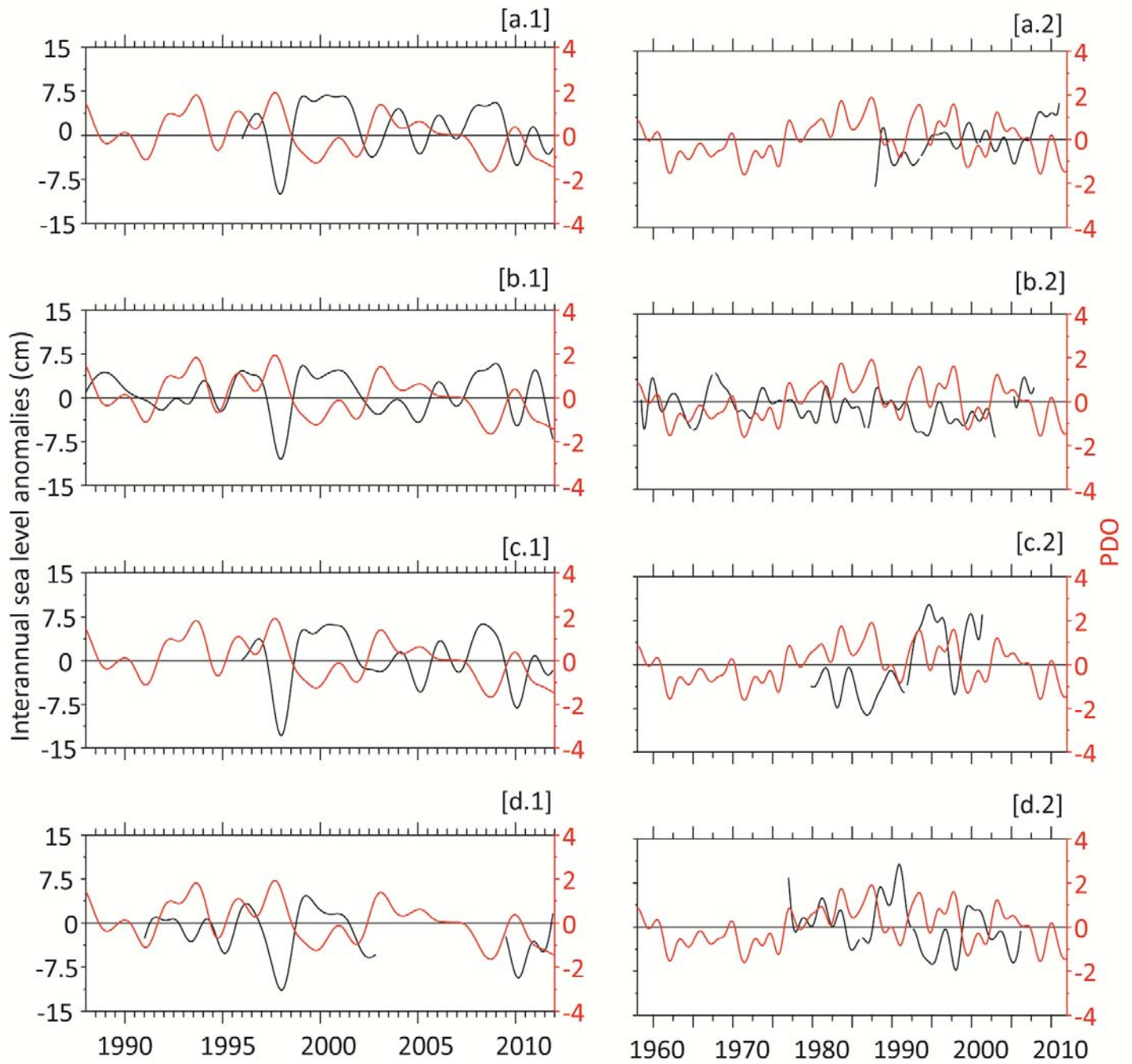


Fig. 7. Spatial correlation pattern of inter-annual sea surface height anomalies (1975 – 2010) with PDO index.

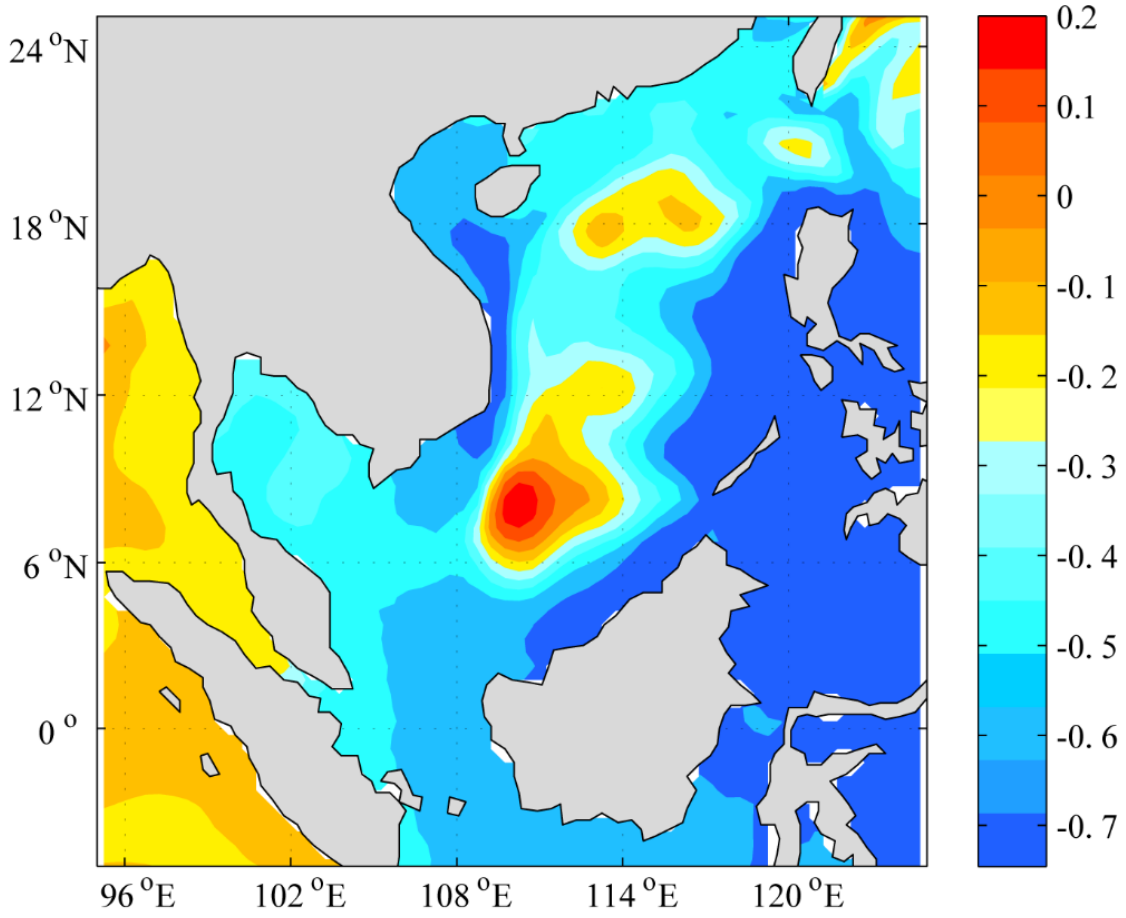


Fig. 8. Wavelet plots of inter-annual sea level anomalies (i) southwest - [a] Sembawang, [b] Sultan Shoal, [c] Tanjong Pagar and [d] Raffles Lighthouse, (ii) southeast- [a] Luban, [b] Kota Kinabalu, [c] Kudat and [d] Peurto Princesa, and (iii) northwest- [a] Getting, [b] Ko Lak, [c] Vung Tau, [d] Qui Nhon

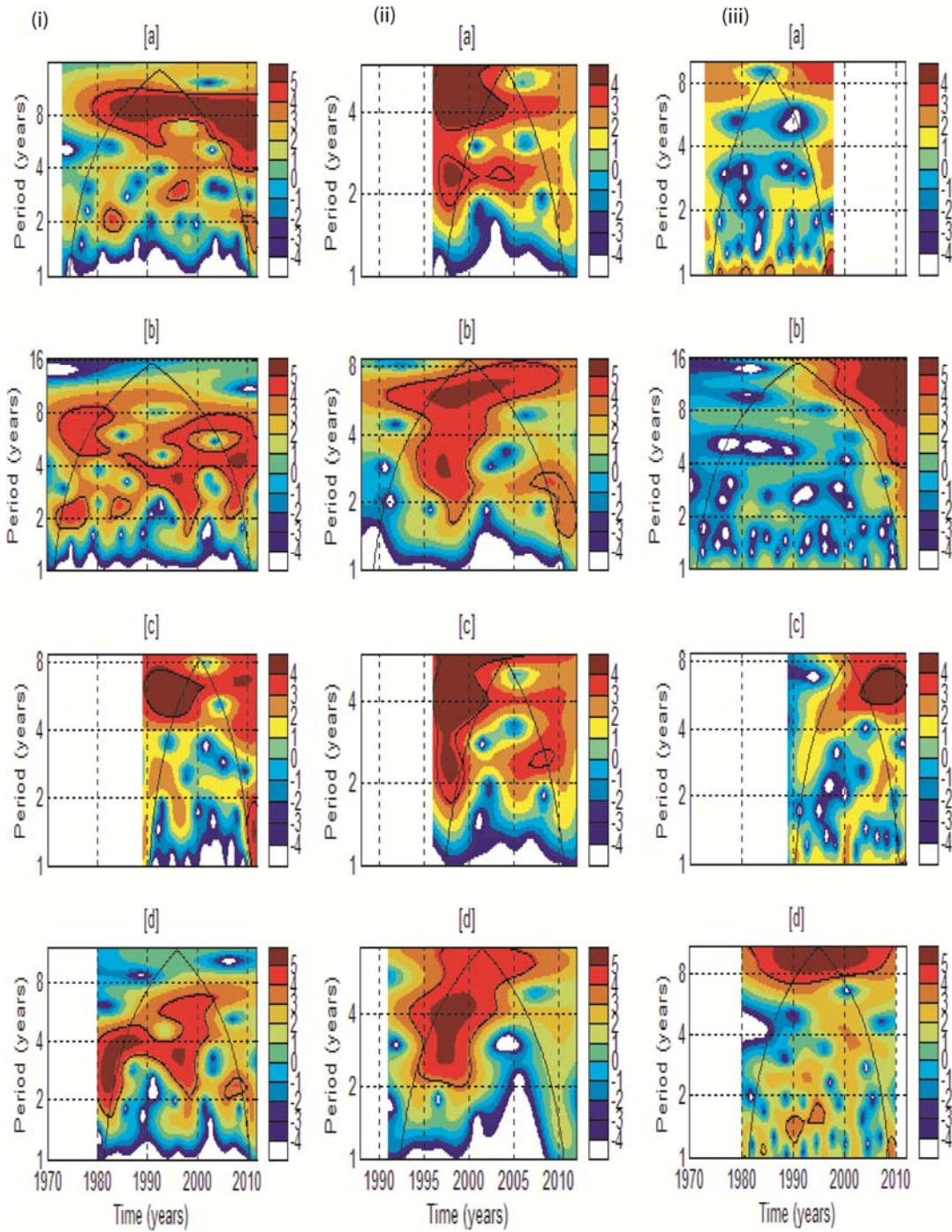


Fig. 9.1. Spatial patterns of EOF, [a] EOF2 and [b] EOF3.

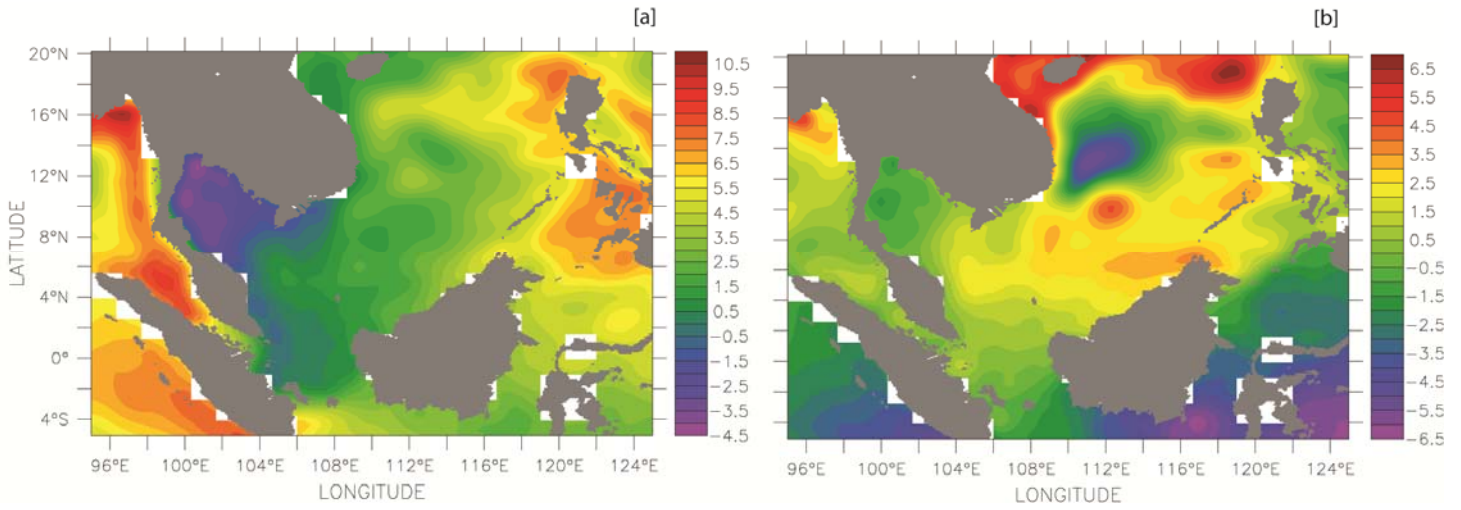


Fig. 9.2. EOF principal components of SLA compared with SOI [a] and DMI [b].

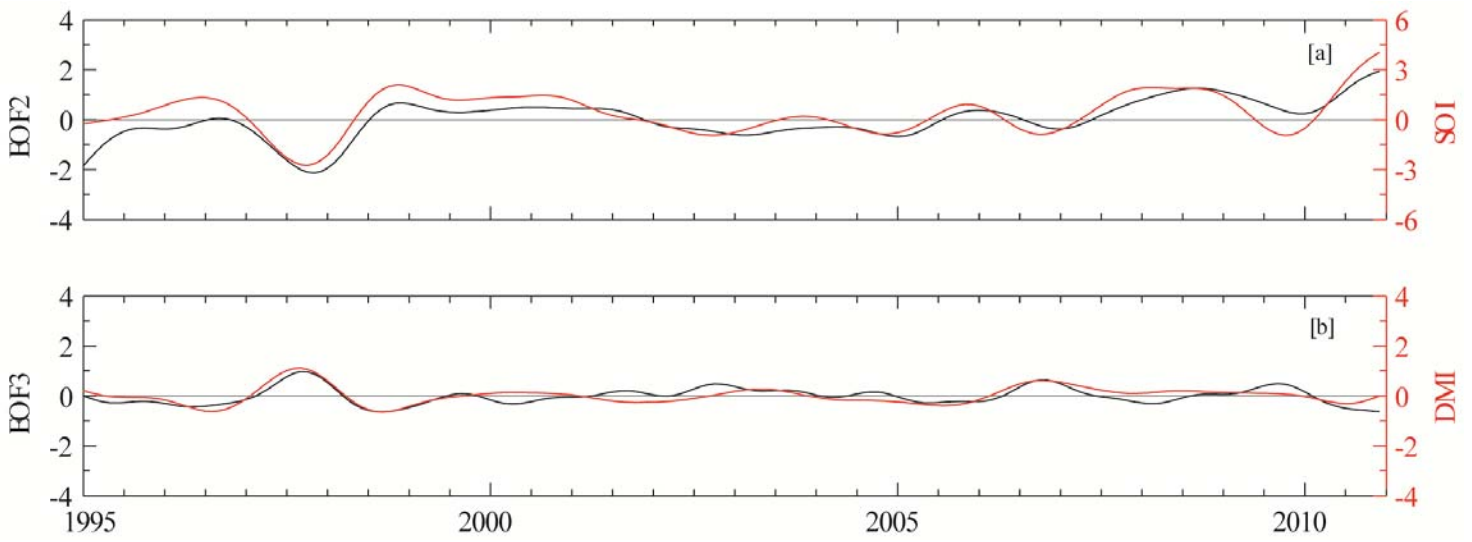




Fig. 10.1. EOF principal component of wind stress curl compared with SOI

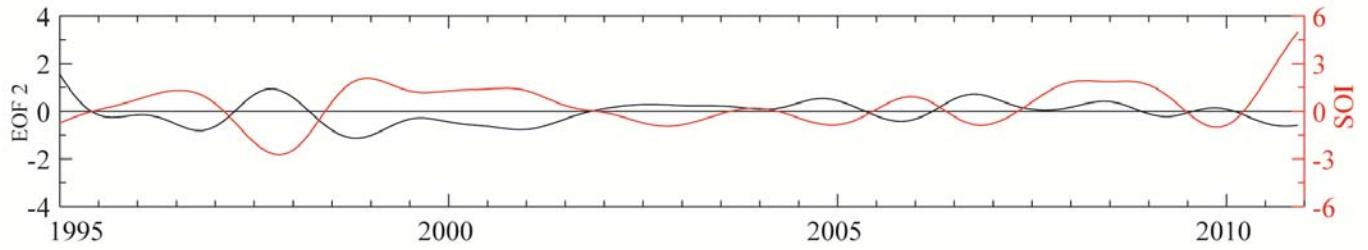


Fig. 10.2. EOF principal component of wind stress curl compared with DMI

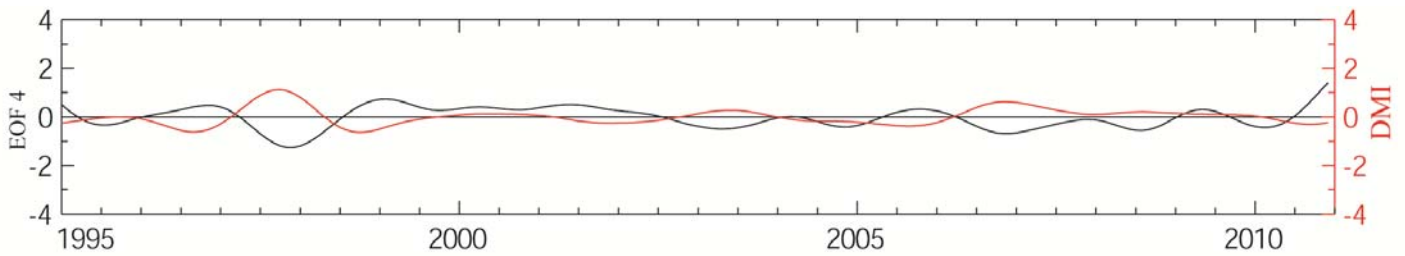


Fig. 11. SLA is compared with SCTF volume transport.

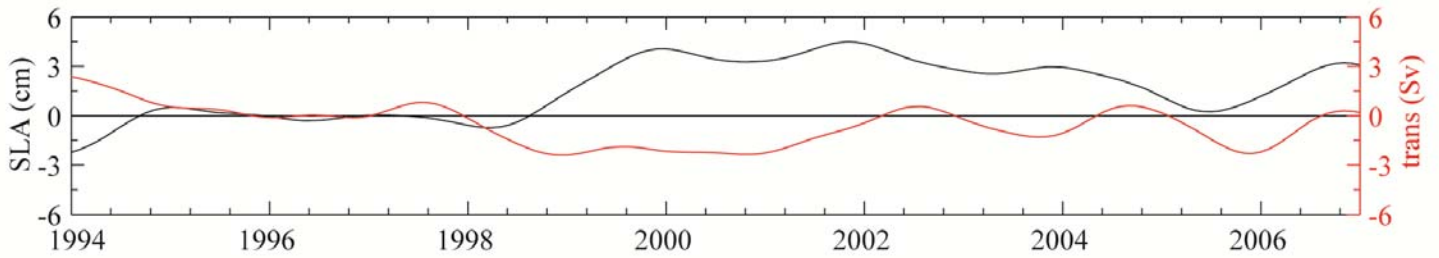


Fig. 12. SCTF volume transport is compared with SOI.

